# Dependence of wind turbine loads on inlet flow field

# Dependence of wind turbine loads on inlet flow field

**Ø. W. Hanssen-Bauer[1], J. B. de Vaal[1,2], M. Tutkun[1], H. Asmuth[3], S. Ivanell[3] and R. Stenbro[1]**

[1] Institute for Energy Technology (IFE), Instituttveien 18, 2007 Kjeller, Norway
[2] Department of Civil and Environmental Engineering, Norwegian University of Science and Technology, Høgskoleringen 7a, 7034 Trondheim, Norway
[3] Department of Earth Sciences, Uppsala University, Cramérgatan 3, SE-621 67 Visby, Sweden

E-mail: oyvind.hanssen-bauer@ife.no

**Abstract.**

In wind farm simulations, the inflow wind field plays a crucial role in the accuracy of both power production, structural load predictions and the turbulent wake development behind wind turbines. Three different inflow wind field generation techniques, namely the Mann model, a reduced order based model described herein and LES data, are used in this study to characterise the relation between the inflow and the structural response of the wind turbine. In addition, the wake development under different inflow conditions are studied. The turbulence statistics of the reduced-order model and the LES data are similar to each other while the Mann turbulence has different turbulence profiles and spectral characteristics. An in-house developed aeroelastic code, 3Dfloat, is used for structural response analysis. The differences between the inflow fields are mainly attributed to the turbulence intensity profiles, and differences in their spectral characteristics.

## 1. Introduction

In wind farm simulations, the inflow wind field plays a crucial role in the accuracy of both power production, structural load predictions and the turbulent wake development behind wind turbines [1, 2]. Organised large scale motions in the Atmospheric Boundary Layer (ABL) and the turbulent wake behind wind turbines affect performance of wind turbines, power production and the turbine life-time directly. Most engineering models are developed for efficiency and speed for streamlined design processes and operation. Therefore, they often lack a complete time and space variation of the turbulence, in particular the energy carrying large scale structures. This leads to uncertainty in spectrum of turbulence kinetic energy and hence the coherence. The large scale motions are responsible for nearly all flux of energy from above the turbine canopy and production of turbulence kinetic energy, and therefore should be accounted for properly in order to minimise uncertainty in wind farm simulations.

Large scale motions are the main contributor to structural loading and flow characterisation behind the wind turbines [2]. Wind turbine wakes behind individual turbines interact with each other in an array configuration. In addition, they interact with the atmospheric boundary layer and therefore the wakes are often far from symmetric. Evolution of the wakes behind the wind turbines are influenced greatly by this interaction, in particular due to the large scale motions.

Structural loading on wind turbines are calculated using aeroelastic simulation codes, and these codes take inflow wind field as input. Recent advances in wind turbine technology, bigger

offshore installations and larger turbines create challenges for the current inflow wind field generators. This is because the new generation offshore wind turbines can reach above the so-called surface layer, which is a fundamental assumption for widely used inflow generators. We assess the effect of inflow on both wake development and structural loading by comparing the Mann model which is the most widely used turbulence generator, a reduced order model which has no surface layer assumption, and Large-Eddy Simulation (LES).

This paper investigates the characteristics of structural loading on wind turbines and sensitivity of turbine wake evolution in different inflow wind field conditions. This is achieved by comparing the widely used Mann turbulence box, a reduced order approach, and velocity planes sampled from a wall-modelled LES of a fully developed neutral atmospheric boundary layer. Previous studies have shown that synthetic turbulence models and LES generated inflow gives comparable results in terms of turbine and wake response [3], and extreme and fatigue loads [4]. In this study, special attention is given to assessment of the uncertainty level as a function of both scale dependence and model selection. The inflow model dependency is investigated by comparing wake-characteristics, power and loads of two inline NREL 5 MW turbines. As an additional reference the same test case is simulated using LES and the Actuator Line Model (ALM) [5].

## 2. Methodology

In this study, we couple the aero-servo-hydro-elastic code, 3DFloat [6], to the flow field in a wind farm. This flow field is based on the Dynamic Wake Meandering (DWM) model [7, 8], that divides the modelling of the wind turbine wake into three individual parts. First, the steady wake is calculated from the thin shear layer approximation to the Navier-Stokes equations in the absence of an axial pressure gradient [9]. Secondly, the wake is meandered by assuming the wake acts as a passive tracer in the cross-wind directions moved by the turbulent boundary layer. The third part of the DWM model, which is used to enhance the turbulence intensity by adding the turbulence coming from the wake to the incoming wind, is not included in this work.

The steady wake model developed by Ainslie [9] and adapted in the DWM model is based on the thin shear layer approximation of the Navier-Stokes equations in the absence of an axial pressure gradient, given by:

$$u_x \frac{\partial u_x}{\partial x} + u_r \frac{\partial u_x}{\partial r} = -\frac{1}{r}\frac{\partial}{\partial r}\left(r\overline{u'_x u'_r}\right). \tag{1}$$

Here $u_x$ and $u_r$ denote instantaneous velocities in $x$ and $r$ directions, respectively. The dash ($'$) and overbar ($\bar{}$) represent fluctuations and ensemble averaging, respectively. It is assumed that the Reynolds stress term $\overline{u'_x u'_r}$ can be obtained using the eddy-viscosity model:

$$-\overline{u'_x u'_r} = \varepsilon \frac{\partial u_x}{\partial r}, \tag{2}$$

where the eddy viscosity, $\varepsilon$, can be divided into two parts; the first part representing the contribution from the ambient boundary layer, $\varepsilon_a$, and the second part representing the contribution from the shear caused by the turbine wake, $\varepsilon_w$:

$$\varepsilon = \varepsilon_a + \varepsilon_w = \frac{\kappa T I U_0 z}{2.4} + 0.015 r_w (U_0 - u_c(x)), \tag{3}$$

where $\kappa \approx 0.4$ is the von Karman constant, $TI = u'_x(Z_0)/U_0$ is the turbulence intensity of the ambient flow at hub height $Z_0$, $U_0$ is the mean flow at $Z_0$, $r_w$ is the wake radius and $U_0 - u_c(x)$ is the velocity deficit at the centerline of the wake for a given streamwise ($x$) position. Together with the continuity equation this result in the following set of equations:

$$u_x \frac{\partial u_x}{\partial x} + u_r \frac{\partial u_x}{\partial r} = \frac{1}{r} \frac{\partial}{\partial r} \left( r\varepsilon \frac{\partial u_x}{\partial r} \right) \tag{4}$$

$$\frac{\partial u_x}{\partial x} + \frac{1}{r} \frac{\partial}{\partial r} (r u_r) = 0 \tag{5}$$

The governing equations are of parabolic type, i.e. information only travels along the characteristic lines parallel with the domain's *temporal* dimension.

The initial axial velocity distribution at the end of the near wake is estimated by the Blade Element Momentum (BEM) model with Prandtl's tip loss factor and the Glauert correction (see e.g. [10]). The lift coefficients $C_L$ and drag coefficient $C_D$ as functions of angle of attack $\alpha$ are found from look-up tables for each blade element that make up the turbine. The length of the near wake, $x_n$, is calculated from an empirical formula by Vermeulen [11].

Meandering of the wake is treated as the wake being a passive scalar which is transported in space by the background turbulent velocity field averaged over the rotor area. Meandering is assumed to happen only in $y$ and $z$ direction, while in $x$ direction the wake is assumed to move with 80% of the free stream velocity, as suggested by [12].

### *2.1. Inflow models*

Three different turbulence boxes, the widely used Mann turbulence box, a reduced order approach based on wind tunnel measurements and a LES of a neutral atmospheric boundary layer, are used as input to 3DFloat for aeroelastic simulations. The velocity fields from the two latter approaches include a mean shear flow, as seen in figure 1, while the synthetic turbulence in the Mann turbulence box include only the fluctuating component that average to zero. The mean velocity profile from the reduced order model is scaled to match the LES mean velocity at hub height (indicate by the middle horizontal line), but the two vertical velocity profiles deviates for high elevation, especially for $z > 150$ meters. Even though the largest deviations between the velocity profiles are found above the height of the turbine, indicated by the upper horizontal line, it was chosen to use the same velocity profile for all the aeroelastic simulations to isolate the effect of the different turbulence boxes obtained from the three models. The mean velocity profile used in the aeroelastic simulations together with the turbulence boxes is a logarithmic profile fitted to the time averaged LES velocity profile:

$$u_x(z) = 1.17 \log(z) + 5.01 \tag{6}$$

This profile is also plotted in figure 1, showing a good match with the LES velocity profile.
In addition to using the same velocity profiles, the boxes are also scaled to have matching turbulence intensities at hub height averaged in lateral direction.

All three inflow models utilise the Taylor's frozen turbulence hypothesis to convert the axial spatial dimension $x$ to the time dimension $t$. For a given mean convection velocity $U$, the frozen field assumption yields:

$$u_i(x, y, z, t + \tau) = u_i(x - U\tau, y, z, t), \tag{7}$$

where $i$ is the index notation ($i = x, y, z$) and $\tau$ denotes the separation in time representing difference between two consecutive samples.

*2.1.1. Mann turbulence* The Mann model [13, 14] generates synthetic turbulent fields based on a spectral tensor developed for atmospheric surface layer turbulence at high wind speeds. The model is based on linearized Navier-Stokes equations and modelled turbulent eddy lifetimes. As detailed in [13, 14], turbulence statistics up to second order can be obtained. The flow is

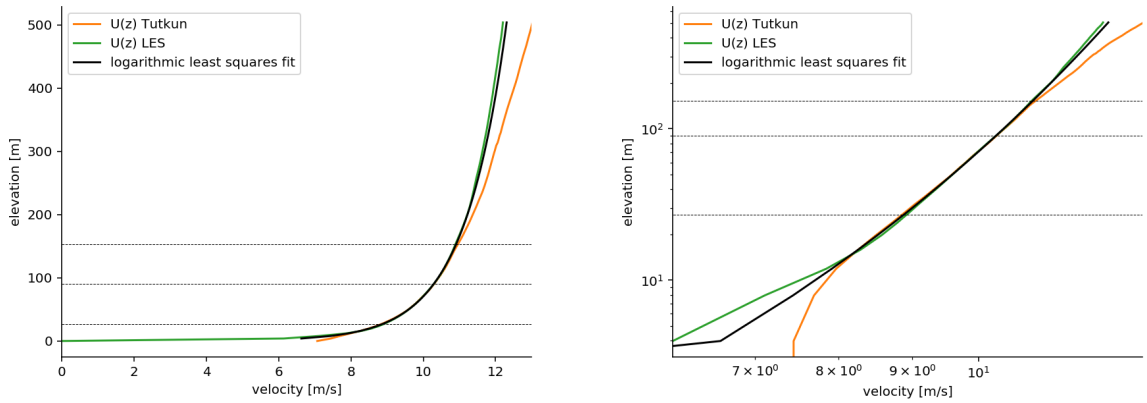


Figure 1: Vertical velocity profiles $U(z)$ from the reduced order model, LES precursor and the logarithmic profile given in equation 6 in $(a)$ linear and $(b)$ logarithmic scale. The horizontal dashed lines indicate the hub height $Z_0$ and the upper and lower blade tips.

incompressible and turbulence is assumed to be isotropic, following the von Karman energy spectrum.

For incompressible isotropic turbulence the spectral tensor is given by

$$\mathbf{\Phi_{ij}}(\mathbf{k}) = \frac{E(k)}{4\pi k^4}(\delta_{ij}k^2 - k_i k_j). \tag{8}$$

where $k$ is the wave number, $\delta_{ij}$ is the Kronecker delta and $E(k)$ is the von Karman energy spectrum:

$$E(k) = \alpha\varepsilon^{2/3}L^{5/3}\frac{L^4k^4}{(1+L^2k^2)^{17/6}}. \tag{9}$$

Here $L$ is the characteristic length scale for the turbulence of the spectral velocity tensor, $\alpha$ is the Kolmogorov constant set to 1.7 and $\varepsilon$ is the turbulence dissipation rate.

There are three parameters in the Mann model that can be adjusted to obtain a desired turbulence field: (i) the characteristic turbulence length scale $L$, (ii) the anisotropy parameter of the sheared spectral tensor $\Gamma_a$ and (iii) $\alpha\varepsilon^{2/3}$. When $\Gamma_a = 0$, the turbulence is isotropic, while for $\Gamma_a > 0$, we have $\sigma_u^2 > \sigma_v^2 > \sigma_w^2$ and $\langle uw \rangle < 0$. As $\Gamma_a$ gets larger, anisotropy within the field increases, hence the difference between the velocity components. Magnitude of the turbulence within the field is measured using the dissipation, since this can be expressed by the turbulence intensity $TI$:

$$\alpha\varepsilon^{2/3} = \frac{4\Gamma(17/6)}{\sqrt{\pi}\Gamma(1/3)}\left(\frac{U_0 TI}{L^{1/3}}\right)^2 \tag{10}$$

(Note that $\Gamma$ is the Gamma function and should not be confused with the anisotropy parameter $\Gamma_a$).

*2.1.2. Reduced order based inflow model.* The reduced-order based inflow model (named Tutkun herein since the measurement data were presented in [15]) is based on reduced order field generation, combining proper orthogonal decomposition (POD) and linear stochastic estimation (LSE) methods. We use turbulent boundary layer wind tunnel data obtained with synchronised hot-wire and stereo-PIV systems.

The POD provides an optimum deterministic description of the field by using deterministic eigenfunctions. These are the solutions obtained once the projection onto the stochastic velocity field of turbulence is maximised in a mean square sense. Maximisation of the projection results in an integral value problem for which the kernel is the two-point cross-correlation tensor of the velocity field. The POD has been found to very efficiently extract the most energetic modes of the flow and order them according to their energy content [16].

In order to obtain a velocity field that is highly resolved in both space and time, LSE is used to combine the temporally highly resolved hot-wire data and the spatially highly resolved PIV data [17]. The result is a three-dimensional box of data for which both space and time are properly resolved. The data used in this paper comes from measurements on a turbulent boundary layer with a free stream velocity of about 10 m/s and a Reynolds number based on momentum thickness of 19,100. The PIV planes are recorded at 4 Hz and consist of $163 \times 141$ spatial points with a spacing of $\Delta z = \Delta y = 2$ mm. The planes cover an area of approximately $\delta \times \delta$ in vertical and spanwise directions, where $\delta$ is the boundary layer thickness. The hot-wire probes are placed in a $11 \times 13$ rake covering the same plane of $\delta \times \delta$ just 1 cm downstream of the PIV planes, and has a recording rate of 30 kHz. The PIV measurements are thus more detailed in space while the time resolution is much higher at the hot-wire points. Further details can be found in Tutkun et al. [15].

To represent the ABL, the wind tunnel data were scaled with a scaling factor of 2000 resulting in $\Delta y = \Delta z = 4$ m, and $f = 15$ Hz giving $\Delta x = U_e/f = 0.68533$ m at the hub height once Taylor's frozen field hypothesis is applied. In the current study, only the high frequency part of the complete spectrum was reduced without keeping all spatial modes in place. To do this a 6th order Butterworth low-pass filter with zero-phase filtering was designed and applied to preserve waveforms of the unfiltered velocity signal. The cut-off frequency was set to be 1 kHz in the wind tunnel scale, which translates to 0.5 Hz in the ABL scale. Filtered hot-wire data was then combined with PIV data using linear stochastic estimation. The cut-off frequency was adjusted to only filter out the components whose contribution to structural loading is minimal, if not completely negligible [4].

*2.1.3. Large-eddy Simulations* For the LES reference case we apply the numerical framework EllipSys3D [18, 19, 20]. The solver has been used in numerous wind power related studies including several fundamental investigations of ABL flows as well as the ALM [5, 21, 22].

The governing equations are formulated in a collocated finite-volume approach. As in previous studies, e.g. [21], diffusive terms are discretised by second-order central differences while a blend of third-order QUICK (10%) and fourth-order central differences (90%) is applied to the convective terms. The pressure correction is solved using the SIMPLE algorithm. Pressure decoupling is avoided using the Rhie-Chow interpolation. As a sub-grid scale model we employ the formulation by Deardorff [23].

The inflow velocity planes are generated in a bi-periodic precursor simulation of a neutral atmospheric boundary layer. The domain measures $1280\,\mathrm{m} in the vertical and 4536\,\mathrm{m}$ in the lateral and stream-wise directions. The grid is uniform with $\Delta x = 20\,\mathrm{m}$ and $\Delta y = \Delta z = 10\,\mathrm{m}$. At the top we apply a symmetry boundary condition. At the bottom the surface shear-stress is prescribed based on the local instantaneous velocity as well as the logarithmic law given by Monin-Obukhov similarity theory [24]. The flow is driven by a stream-wise constant pressure gradient $\partial p/\partial x = -\rho\, u_*^2/L_z$ with a friction velocity $u^* = 0.44\,\mathrm{m/s}$. The surface roughness is set to $z_0 = 0.01\,\mathrm{m}$. Cross-sectional planes of the velocity field are sampled after a fully turbulent boundary layer has developed.

For comparison of the wakes obtained from DWM with different inflow fields, additional LES where performed, referred to as full LES. On this account, the pre-generated velocity planes where inserted in a successor simulation including wind turbines represented by the ALM. The

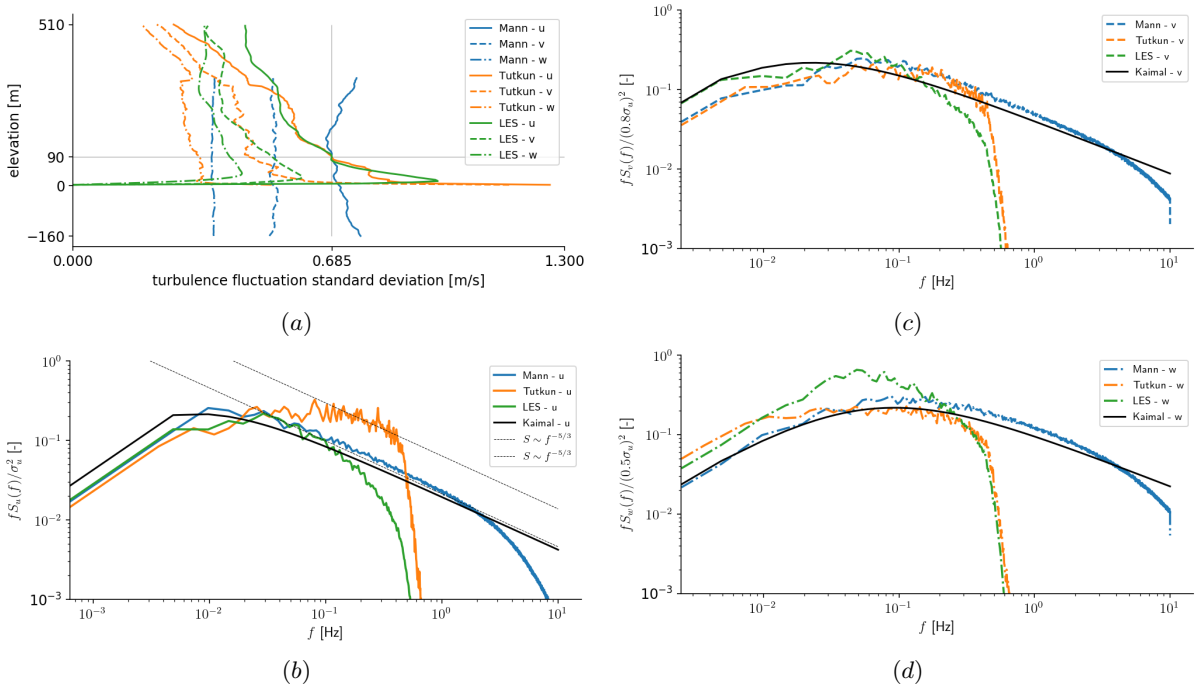


Figure 2: Comparison between Mann inflow models, the reduced order model (Tutkun) and LES precursor ($a$) standard deviations, and turbulence spectra of ($b$) streamwise ($x$) ($c$) spanwise ($y$) and ($d$) vertical ($z$) velocity components.

extent of the domain is identical to the precursor. The first turbine is located $6D$ downstream of the inlet. The finest region of the grid is uniform with a cell width $\Delta x = \Delta y = \Delta z = D/32$ starting $3D$ upstream of the turbine and extending up until $21D$ downstream of the turbine. It comprises $4D$ in the lateral and vertical direction. Outside of the inner region the grid is continuously stretched towards the boundaries. The total grid encompasses $36.9 \cdot 10^6$ cells.

### *2.2. Test case*

Two NREL 5MW reference turbines [25] at a spacing of $7.5D$ apart in a row align with the mean wind direction are used in this study. These turbines has hub height $Z_0 = 90$ m, rotor diameter $D = 126$ m, rated speed $U = 11.4$ m/s and rated tip speed ratio $TSR = 7.55$. The wind speed at the hub height is $U_0 = 10.28$ m/s, and all the turbulence boxes are scaled to a turbulence intensity of $TI = 6.65\%$ at the same location.

## 3. Results

In this study we performed calculations on the aeroelastic performance on the wind turbines using the in-house aeroelastic simulator developed at IFE, called 3DFloat. The simulator can provide any type of force, moment, vibration and fatigue data on the wind turbine. In this section we present the turbulence statistics (3.1), comparison of the turbulent wake behind the turbine (3.2) and loads (3.3).

### *3.1. Turbulence statistics and power production*

Figure 2 ($a$) reveals large differences in the standard deviations of the three inflow models. While the Mann turbulence is almost independent of elevation, the standard deviations of the two other inflow models decrease with elevation. For all inflow models we have $\sigma_u > \sigma_v > \sigma_w$, but the

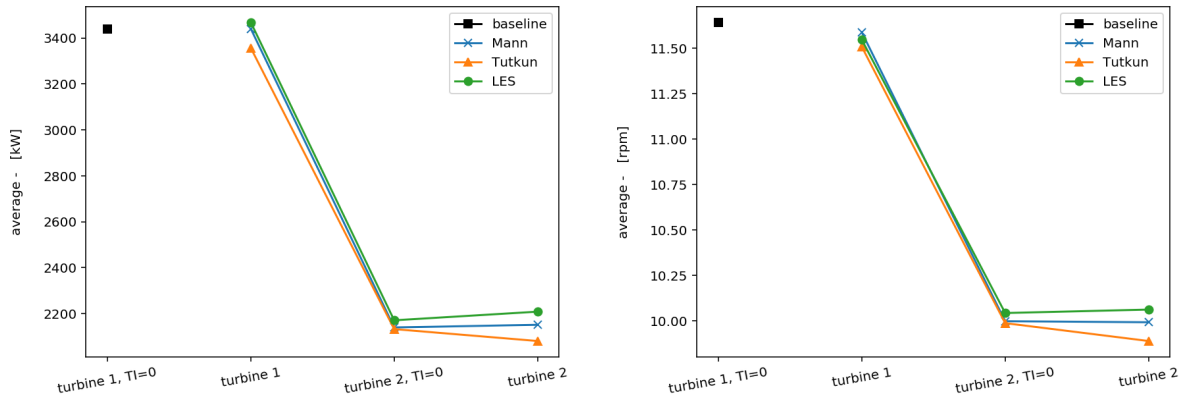


(*a*) (*b*)

Figure 3: (*a*) Power production for three different inflow conditions and (*b*) corresponding mean rotor speed. The different load cases given on the $x$ axis are explained in table 1.

difference at hub height is largest for Tutkun, and smallest for the LES precursor. Figure 2 (*b*), (*c*) and (*d*) shows the frequency spectra of the streamwise), crosswise and vertical component of the fluctuating part of the velocity for the three inflow models at hub height. In addition, the Kaimal spectrum is plotted in black. The spectra are normalised by $\sigma_u^2/f$, $0.8\sigma_u^2/f$ and $0.5\sigma_u^2/f$ for the streamwise, crosswise and vertical component, respectively, where $\sigma_v = 0.8\sigma_u$ and $\sigma_v = 0.5\sigma_u$ are taken from the IEC standard for the Kaimal spectrum. All the inflow models follow the Kaimal spectrum reasonably well, but while the Tutkun and LES precursor turbulence contains energy up to around 0.5 Hz, the Mann turbulence contains energy up to around 5 Hz. Turbulence field obtained using the reduced order approach (Tutkun) contains more energy between 0.1 Hz and 0.5 Hz compared to the two other inflow models for the axial velocity component $u$, while the LES precursor contains more energy for the transverse velocity components around 0.01 to 0.1 Hz compared to Mann and Tutkun. Note that the sharp roll-off of the Tutkun spectrum is due to removing all high frequency contribution from the velocity field by applying the low-pass filter. A similar roll-off in the LES spectra is also visible, especially for the streamwise component. The roll-off seems to be begin a bit earlier in the LES case and this could be attributed to the spatial filtering introduced by the grid cell size.

Figure 3 shows mean power production and rotor speed achieved from four different load cases. First we have a baseline case, where a turbine is exposed to a shear flow equal to the logarithmic profile shown in figure 1, and without any background turbulence in terms of a turbulence box (i.e. $TI = 0$). This case is called "turbine 1, $TI = 0$". For the second case a turbine is exposed to a shear flow plus a turbulence box with $TI = 6.65\%$. This case is called "turbine 1". For the two last cases a turbine is exposed to a shear flow with a deficit from the wake of turbine 1 positioned $7.5D$ upstream, superimposed. The wake of turbine 1 is meandered by the in terms of a turbulence box with $TI = 6.65\%$. For the third load case, called "turbine 2, $TI = 0$", the turbine is exposed to this inflow alone, while for the fourth case this inflow is combined with a turbulence box with $TI = 6.65\%$. All the load cases, except the baseline case "turbine 1, $TI = 0$", has three variations as they are run with the different turbulence boxes generated as described in section 2.1. The different load cases are summarised in table 1.

As expected, power production is decreased from turbine 1 to turbine 2 due to the decreased mean incoming wind speed. Also the mean rotor speed is lower as it is decreased by the controller to obtain the rated TSR. The incoming turbulence intensity has less impact on the power

Table 1: Inflow conditions for the different turbine cases

| | turbine 1, $TI = 0$ (baseline case) | turbine 1 | turbine 2, $TI = 0$ | turbine 2 |
|---|---|---|---|---|
| Shear flow (equation 6) | × | × | × | × |
| Background turbulence | | × | | × |
| Meandered wake deficit | | | × | × |

production and rotational speed. There is a slight variation between the different inflow wind fields. This can be attributed to small differences in mean velocities and turbulence intensities at hub height for the different cases. Both Tutkun and the LES based inflow have standard deviation profiles running all the way to the wall where turbulence intensity peaks within the near wall region.

*3.2. Wake comparison*

Figure 4 compares the time averaged wake deficit $u_{def} = U - u$ at different downstream positions obtained from full LES, and four variations of the DWM model; *one* with the absence of wake meandering, i.e. only the axisymmetric wake obtained from equation 4 and 5, and three wakes meandered by the three different turbulence boxes. The top and bottom row presents the spanwise and vertical wake profiles, respectively. The two turbines are placed at $x/D = 0$ and $x/D = 7.5$. At $x/D = 2.5$, different simulations yield typical near-wake profiles, with two peaks in the velocity deficit near the rotor blade tip ($y/D = \pm 0.5$ spanwise, and $z/D = 0.21$ and $z/D = 1.21$ vertically). At this downstream position the wake obtained from full LES has a noticeably lower deficit than the the DWM wakes, and it also has a clear asymmetry, i.e. having a higher deficit above hub height and also at the right half of the wake when looking downstream ($y < 0$). As the wake develops downstream, the shape of the velocity deficit becomes approximately Gaussian, as seen at $x/D = 5$. At the same time, the wake expands while the maximum deficit decays. Here, the difference between the wake obtained from full LES and the DWM wake is smaller. For $x/D > 7.5$, the velocity deficits are a result of the combined wakes from the two turbines. At $x/D = 10$, which is a distance $2.5D$ behind the second turbine, the deficits have increased in magnitude since turbine 2 has extracted energy from the wind. Here the shapes of the wake obtained from full LES and the DWM wake are fundamentally different. While the DWM wake has similar shape to position $x/D = 2.5$, the wake obtained from full LES has already developed to an approximately Gaussian shape. This difference is probably related to an increased turbulence felt by turbine 2 being in the wake of turbine 1. This causes the wake obtained from full LES of turbine 2 to develop faster than turbine 1, while for the DWM simulations this effect is not captured. Further downstream positions as the wakes develop the difference in both shape and magnitude of the wakes obtained from full LES and DWM are getting smaller. On the other hand, while the DWM wakes stay symmetric, the ground limits a free expansion of the lower part of the wake obtained from full LES. Also the spanwise profile of the wake obtained from full LES is clearly asymmetric about $y/D = 0$. This is probably due to a small non-zero spanwise component in the incoming flow of the full LES.

In general, there are only small differences when comparing the shapes of the time averaged wake deficits obtained from different DWM simulations. There is, however, some differences as the time averaged meandered wakes are wider and has a lower velocity deficit compared to the non-meandered wake, and this effect is largest for the wake meandered by the LES precursor. This can be seen from table 2, containing the maximum velocity deficits for the different cases. The fact that the wake is meandering more when exposed to the LES turbulence

Table 2: Maximum velocity deficit [m/s]

| | $x/D = 2.5$ | $x/D = 5$ | $x/D = 10$ | $x/D = 12.5$ | $x/D = 15$ |
|---|---|---|---|---|---|
| Full LES | 5.09 | 3.79 | 5.61 | 3.61 | 2.60 |
| No meandering | 5.59 | 4.34 | 5.59 | 4.34 | 3.06 |
| Mann meandering | 5.53 | 4.18 | 5.53 | 4.18 | 2.87 |
| Tutkun meandering | 5.54 | 4.17 | 5.54 | 4.17 | 2.83 |
| LES meandering | 5.46 | 4.03 | 5.46 | 4.03 | 2.71 |

is probably a result of slightly more energy at the lower frequencies important for meandering ($f < \sim U_0/D \sim 10^{-1}$ Hz), for the spanwise and vertical components of this turbulence (see figure 2*c* and 2*d*).

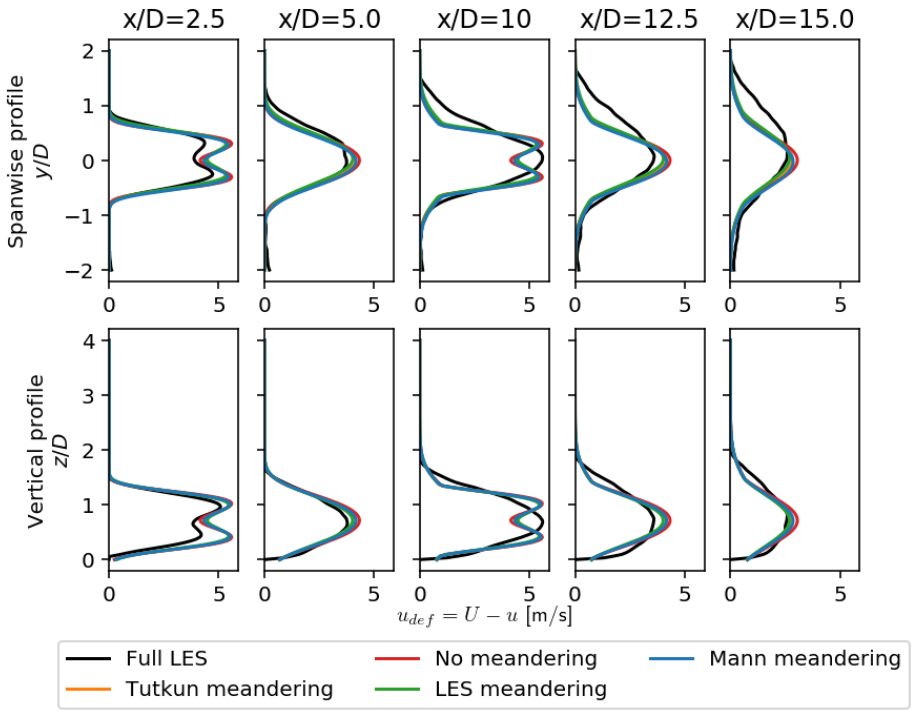


Figure 4: Wind turbine wake development behind the turbine.

*3.3. Loads*

Figure 5 shows damage equivalent loads (DEL) for the cases given in table 1, when varying the inflow models. Figure 5 (*a*), (*b*) and (*c*) present tower base fore-aft bending moment, blade root flapwise bending moment and yaw bearing torsional moment, respectively. As seen in figure 5, the results indicate that the damage equivalent loads are highly dependent on the inflow model. The LES inflow model gives in general lower loads than the Mann model, while the inflow model using a reduced order approach (Tutkun) gives even higher loads. The loads on the turbines exposed to a turbulent inflow are considerably higher than the cases with $TI = 0$, while the different turbine cases with a similar $TI$ at the inlet experience loads at the same level. This

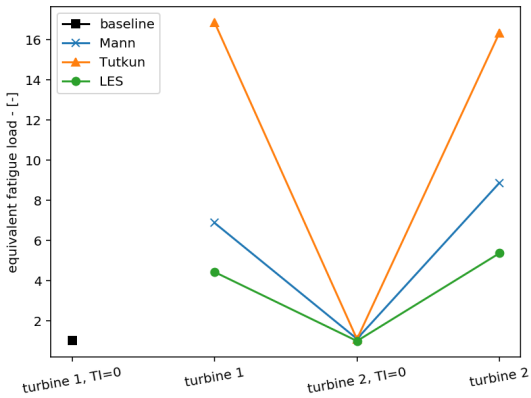


(*a*) Tower base fore-aft bending moment.

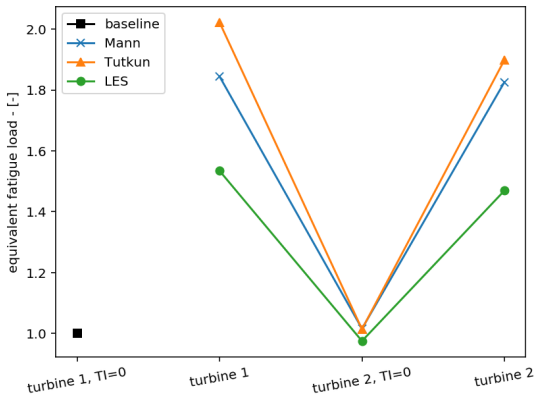


(*b*) Blade root flapwise bending moment.

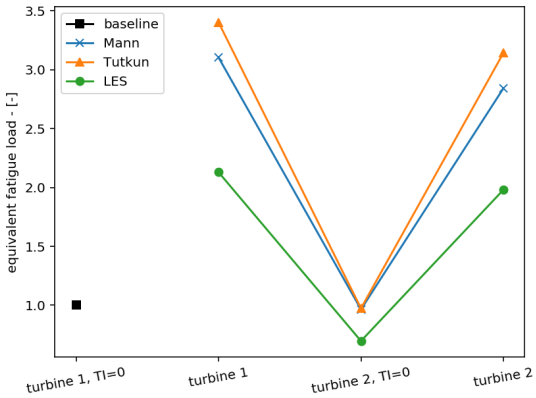


(*c*) Yaw bearing torsional moment.

Figure 5: Comparison of damage equivalent loads between the baseline, Mann model, LES and reduced order model. The different load cases given on the $x$ axis are explained in table 1.

suggests that the effect of the atmospheric turbulence interacting with the turbine has a higher contribution to the loads compared to turbulence introduced by the meandered wake from an upstream turbine.

Figure 6 shows spectra of structural response of the turbines. The frequency response of the tower base fore-aft bending moment shown in figure 6 (*a*) reveals that the inflow model using the reduced order approach (Tutkun) in general gives higher loads than the Mann model. With Tutkun turbulence the loads have a peak in the spectra at a frequency corresponding to the two lowest natural frequencies of the system, the fore-aft and side-to-side bending moments. The spectra for the Mann model, however, have its peak at a higher frequency, corresponding to the 3P frequency of the rotor ($\sim$ 0.58 Hz for turbine 1 and $\sim$ 0.5 Hz for turbine 2). This can be explained by the fact that there are more energy at low(er) frequencies in the reduced order turbulence compared to Mann and the LES precursor. For Mann and the LES precursor, the presence of the wake increases the load peak and shifts the frequency towards the tower modes, resulting in higher damage equivalent loads. For the reduced order turbulence, the frequency spectrum, and also the damage equivalent loads (DEL), are not affected significantly by the wake.

For the blade root flapwise bending moment, the load response peaks correspond closely to

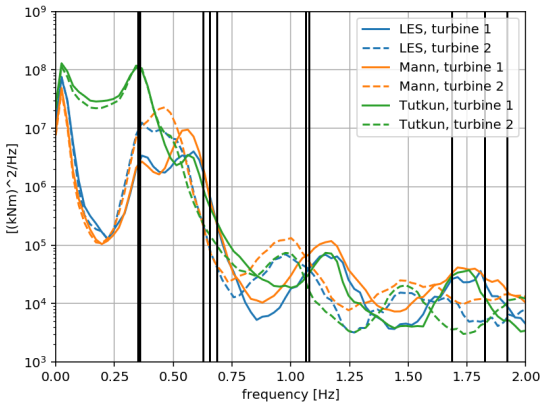


(*a*) Tower base fore-aft bending moment

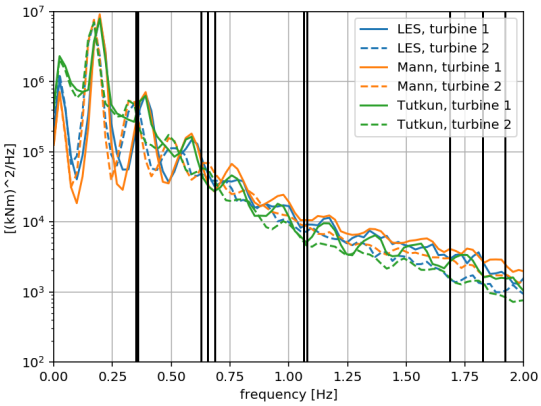


(*b*) Blade root flapwise bending moment

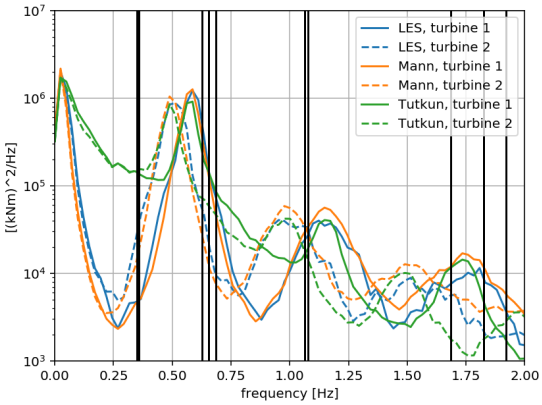


(*c*) Yaw bearing torsional moment

Figure 6: Comparison of spectra between the inflow wind models. The vertical, black lines show the eigenfrequencies of the NREL 5MW turbine.

the 1P natural frequency, while for the yaw bearing torsional moment, the peaks correspond to the 3P frequency. No significant difference between the inflow models are seen for the peaks. However, the loads are in general seen to be larger for the reduced order model, resulting in higher DEL.

The spectra of yaw bearing torsional moment show that load response peaks correspond closely to the 3P frequency. Due to lower average wind speed when operating in the wake deficit, the 3P frequency is correspondingly lower, and moves further away from the collective blade natural frequencies.

## 4. Conclusions

The results presented herein are taken from an ongoing research recently financed by the Norwegian Research Council to develop tools that are both very accurate and fast for simulating the loads and performance for wind turbines in a farm configuration. Our findings in neutral atmospheric conditions, mean wind velocities of about 10 m/s and turbulence intensity of 6.65%, indicate that there are non-negligible differences between the Mann model, a reduced order model and a LES based inflow model when the structural loading is considered. Some of the differences in structural response is attributed to the differences in spectral characteristics of

different inflows, i.e. the Mann model has isotropic turbulence spectrum while the others have boundary layer turbulence spectra. The reduced order model results in higher damage equivalent loads compared to the others, in particular for the tower base fore-aft bending moment.

## 5. Funding and acknowledgments

This work has been funded by the Norwegian Research Council, through the project NEXTFARM - Engineering speed modelling of realistic fatigue for all the individual turbines in wind parks by representative pre-calculations, Grant No. 281020.

## References

[1] Bastine D, Vollmer L, Wächter M and Peinke J 2018 *Energies* **11** 612
[2] Saranyasoontorn K and Manuel L 2008 *Journal of Wind Engineering and Industrial Aerodynamics* **96** 503–523
[3] Shaler K, Jonkman J, Doubrawa Moreira P and Hamilton N 2019 FAST. Farm Response to Varying Wind Inflow Techniques Tech. rep. National Renewable Energy Lab.(NREL), Golden, CO (United States)
[4] Sim C, Basu S and Manuel L 2012 *Energies* **5** 2071–2092
[5] Sørensen J N and Shen W Z 2002 *J. Fluids Eng.* **124** 393–399
[6] Nygaard T A, De Vaal J, Pierella F, Oggiano L and Stenbro R 2016 *Energy Procedia* **94** 425–433
[7] Larsen G C, Madsen H A, Thomsen K and Larsen T J 2008 *Wind Energy: An International Journal for Progress and Applications in Wind Power Conversion Technology* **11** 377–395
[8] Madsen H A, Larsen G C, Larsen T J, Troldborg N and Mikkelsen R 2010 *Journal of Solar Energy Engineering* **132** 041014
[9] Ainslie J F 1988 *Journal of Wind Engineering and Industrial Aerodynamics* **27** 213–224
[10] Hansen M O 2015 *Aerodynamics of Wind Turbines* (Routledge)
[11] Vermeulen P E J 1980 *3rd International Symposium on Wind Energy Systems* pp 431–450
[12] Keck R E, Mikkelsen R, Troldborg N, de Maré M and Hansen K S 2014 *Wind Energy* **17** 1247–1267
[13] Mann J 1994 *Journal of fluid mechanics* **273** 141–168
[14] Mann J 1998 *Probabilistic engineering mechanics* **13** 269–282
[15] Tutkun M, George W K, Delville J, Stanislas M, Johansson P B V, Foucaut J M and Coudert S 2009 *Journal of Turbulence* N21
[16] Tutkun M and George W K 2017 *Physics of Fluids* **29** 020707
[17] Adrian R J 1979 *The Physics of Fluids* **22** 2065–2070
[18] Michelsen J A 1994 Basis3D - a platform for development of multiblock PDE solvers Tech. Rep. Technical University of Denmark, DTU
[19] Michelsen J A 1994 Block structured multigrid solution of 2D and 3D elliptic PDE's Tech. Rep. Technical University of Denmark, DTU
[20] Sørensen N N 1995 *General Purpose Flow Solver Applied to Flow over Hills* Ph.D. thesis Risø National Laboratory Roskilde, Denmark
[21] Troldborg N, Sorensen J N and Mikkelsen R 2010 *Wind Energy: An International Journal for Progress and Applications in Wind Power Conversion Technology* **13** 86–99
[22] Asmuth H, Olivares-Espinosa H, Nilsson K and Ivanell S 2019 *Journal of Physics: Conference Series* **1256** 012022
[23] Deardorff J W 1980 *Boundary-Layer Meteorology* **18** 495–527
[24] Monin A S A M O 1954 *Nauk SSSR Geophiz. Inst* **24** 163–187
[25] Jonkman J, Butterfield S, Musial W and Scott G 2009 Definition of a 5-MW reference wind turbine for offshore system development Tech. rep. National Renewable Energy Lab.(NREL), Golden, CO (United States)